Solid Freeform Fabrication 2023: Proceedings of the 34th Annual International Solid Freeform Fabrication Symposium – An Additive Manufacturing Conference
Reviewed Paper

A comparison of the mechanical behavior of AlSi7Mg alloy produced through additive manufacturing and subjected to different heat treatment and aging conditions

K. Caballero[1,2], V.A. Medrano[1,2], E. Arrieta[1,2], J. Merino[1,2], B. Ruvalcaba[1,2], B. Ramirez[1,2], J. Diemann[5], L. E. Murr [1], R.B. Wicker[1,2], D. Godfrey[4], M. Benedict[3] and F. Medina[1,2]

[1] W.M. Keck Center for 3D Innovation, The University of Texas at El Paso, El Paso, TX 79968, USA
[2] Department of Aerospace and Mechanical Engineering, The University of Texas at El Paso, TX 79968, USA
[3] Air Force Research Laboratory, Wright-Patterson Air Force Base, Dayton, OH, 45433, USA
[4] SLM Solutions NA, Inc. Wixom, MI 48393, USA
[5] SLM Solutions Group AG, Lübeck, Germany

Keywords: AlSi7Mg alloy, Laser powder bed fusion, EOS M290 and SLM 280HL systems, Heat treatments, Microindentation hardness (HV), Mechanical properties analysis

ABSTRACT

The versatility and adaptability of Aluminum F357 (AlSi7Mg) make it a popular material in the aerospace and defense industries. In this study, two different laser powder bed fusion systems, EOS M290, and SLM 280HL were used to create specimens of Aluminum F357. These specimens were subjected to five different heat treatments: As-built, stress relief (SR), hot isostatic pressing (HIP), T6, and HIP+T6) as per ASTM F3318-18 standard. The printed specimens were then reduced to tensile bars through machining and tested for mechanical properties as per ASTM E28 using an MTS Landmark tensile testing system. In addition to the mechanical behavior analysis, the study used a JEOL JSM-IT500 SEM to observe and document the fracture produced by the tensile test and a Qness 30 CHD Master+ microhardness testing system to obtain hardness (HV) values of the alloy. The results showed that specimens fabricated in the Z direction had a tendency for higher yield strengths of approximately 225 MPa and although these results were similar between LPBF systems some variances can still be seen. However, these differences between the LPBF systems were observed to be partially mitigated by heat treatments. In conclusion, this study highlights the significance of heat treatment on the mechanical properties of Aluminum F357. The results provide valuable information for the aerospace and defense industries to optimize their processes and produce high-quality components. The compatibility of LPBF system fabrication and the mitigation of differences observed between LPBF machines by heat treatments, further demonstrate the potential of this method for producing high-quality Aluminum F357 components.

1 INTRODUCTION

Generally, aluminum alloys possess a wide array of desirable engineering characteristics, including low density, high strength, a high strength-to-weight ratio, resistance to corrosion, weldability, and recyclability. Among these properties, strength and related mechanical attributes

such as hardness and elongation can be adjusted to suit various engineering applications through processes like forging, casting, and heat treatment. These processes result in different microstructures, such as grain sizes, dendrite structures, and interparticle spacings, which directly impact the mechanical properties [1-10].
Additive manufacturing, particularly laser powder bed fusion (LPBF), has introduced additional microstructural features in aluminum alloys due to rapid cooling rates [11]. As a result, new possibilities have emerged for manipulating and selecting mechanical properties through post-process heat treatment, particularly for popular alloys like hypoeutectic AlSi10Mg and AlSi7Mg [12-23]. Heat treatment approaches for LPBF-fabricated AlSiMg alloys include stress relief annealing, T6 treatment (solution heat treatment followed by quenching, cooling, and aging), high-pressure T6 treatment, direct aging, hot isostatic processing (HIP), and various combinations and sequences of these treatments at different temperatures and durations [11,14,17,18,21]. These characteristics of LPBF fabrication and post-process heat treatment have expanded the range of applications for AlSiMg alloys, especially in complex component geometries. Examples include structures for impact and energy absorption, heat exchangers with intricate internal cooling channels, and an increasing number of components in electric vehicles and aerospace systems [12,16,22,23].
This study focuses on the post-process heat treatment of LPBF-fabricated AlSi7Mg (F357) alloy and serves as a follow-up to a comprehensive comparison of heat treatments, residual microstructures, and mechanical properties for AlSi10Mg (A356) alloy, which was recently published [24]. Similar to AlSi10Mg, AlSi7Mg alloy finds wide-ranging applications, as briefly mentioned earlier. The novelty and significance of this research lie in the extensive development of mechanical property data, including 1660 measurements of tensile properties (yield strength, ultimate tensile strength, and elongation) and micro indentation hardness (HV) for components fabricated in the build direction (Z) and the load direction perpendicular to the build direction (XY) in their as-built, aged, heat-treated, and aged states. Additionally, this study compares these mechanical properties for AlSi7Mg components fabricated using two different LPBF systems, which is crucial for standardizing the product.

2 MATERIALS AND METHODS

2.1 Powder feedstocks

The powder utilized in the SLM system was atomized F357 (AlSi7Mg) shown in Table 1; supplied by IMR Metal Technologies (Frankfurt am Main, Germany). The powder had a particle size distribution of D10: 26.4 μm, D50: 39.7 μm, and D90: 59.7 μm.

The powder utilized in the EOS system was atomized F357 (AlSi7Mg) shown in Table 1 and Figure. 1 (a) and (b); provided by Valimet, AM 357C (Stockton, California). A Retsch Camsizer X2 (Haan, Germany) was used in order to study particle size and shape of the powder through dynamic image analysis with a two-camera-system, the Camsizer yields consistent particle size distribution and shape analysis. The stock powder had a particle size distribution of D10: 24.4 μm, D50: 39.3 μm, and D90: 60.4 μm.

Table 1. Powder chemical composition (wt.-%)

Alloy	Al	Si	Fe	Cu	Mn	Mg	Zn	Ti	Be	Other elements, each	Other elements, total
F357 (EOS)	Balance	6.5 - 7.5	0.10	0.20	0.10	0.40 - 0.70	0.10	0.04 - 0.20	0.002	0.05	0.15
F357 (SLM)	Balance	7.1	0.08	0.001	0.001	0.56	0.002	0.07	-	-	-

For further analysis, a JEOL JSM-IT500 Scanning Electron Microscope (SEM) was used to produce images and for analysis which revealed minimal porosity and spherical morphology of the powder, shown in Figure 1.

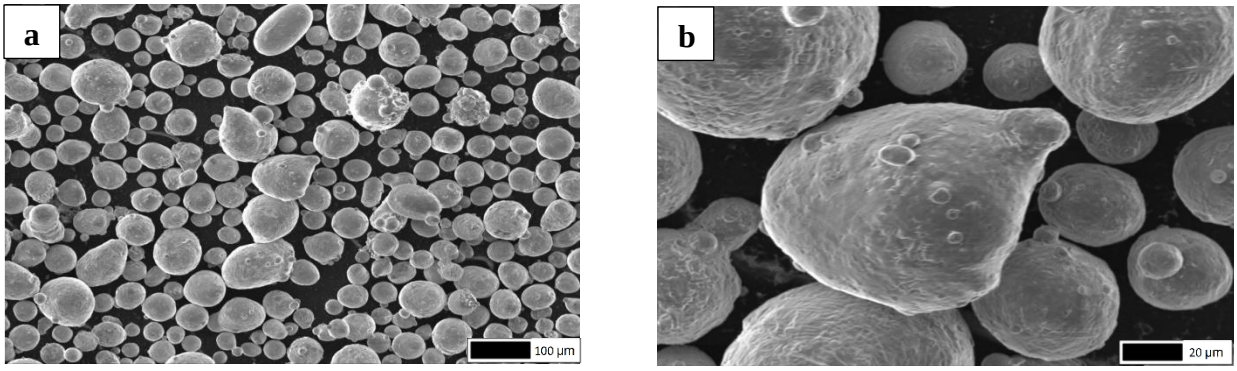

Figure 1. F357 gas-atomized powder SEM images, a) low magnification, b) high magnification

2.2 Laser powder bed fusion systems and process parameters.

In accordance with industry best practices, SLM Solutions, based in Lubeck, Germany, employed an SLM 280HL system with a build size measuring 280 x 280 x 365 mm to manufacture specimens. The F357 alloy was utilized, and the fabrication process involved a laser power of 370 W, a scan speed of 1200 mm/s, and a layer thickness of 30 µm, adhering to the specified parameters.

Furthermore, at The University of Texas at El Paso, printed specimens were produced using an EOS M290 system from Kralling, Germany. This particular system features a 400 W Ytterbium fiber laser and a build volume measuring 250 x 250 x 325. After careful consideration of the experimental design, the F357 alloy was employed in the fabrication process. The parameters utilized were a laser power of 370 W, a scan speed of 1300 mm/s, a hatch of 0.13 mm, and a layer thickness of 30 µm.

2.3 Thermal processing/heat treatment

An ASTM standard for heat-treating additively manufactured aluminum F357 does not currently exist. However, in this study on F357, the ASTM F3318 standard was followed. Previous studies have demonstrated that post-process heat treatments can modify the microstructure and mechanical properties of laser powder bed fusion aluminum F357 parts at room temperature (25 °C). Therefore, this work applied a variety of post-process heat treatments to the F357 specimens. The heat treatments conducted on the F357 specimens included stress relief (SR)

anneals, T6 treatment, hot isostatic pressing (HIP), and combinations of these treatments. Additionally, artificial thermal aging was performed on some specimens to observe changes in microstructure and mechanical properties. Two different aging temperatures (140.5 °C and 177 °C) and three aging times (0 hours, 100 hours, and 1000 hours) were selected. The resulting microstructures were characterized using optical metallography, and the mechanical properties were evaluated through room temperature tensile tests and Vickers micro-indentation hardness measurements. With the application of five heat treatments and five different aging conditions, this study presents results for up to 100 different variants of F357.
Heat treatments consist in use of temperature and time at temperature to modify the properties of a material, in this case printed aluminum F357. The schedules of the heat treatments consist in the aging of as-built F357 samples, one stress relief treatment (SR1), HIP, T6, and HIP+T6 treatments of the printed samples. ASTM F3318 was used for heat treatment standards shown below:

Heat treatments:

SR1: 285°C (±14°C) for 120 min (±15 min), air cooled
HIP: 100MPa, 515°C (±14°C) for 180 min, inert atmosphere cooled
T6: 530°C (±6°C) for 360 min, quenched in water, aged 160°C (±6°C) for 360 min
HIP + T6: HIP, followed by T6 processing

Aging:

Times: 0hr, 100hr, 1000hr.
Temperatures: 140°C and 177°C.

A total of 100 experimental variants were created with these two orientations, times and temperatures as listed in Table 2 and Table 3 below for each of the LPBF systems utilized in this study.
Aging was monitored with external type K thermocouples and recorded by two independent automatic data loggers every 30min to ensure the temperature continue constant at 140°C and 177°C for the 100 and 1000 hours.

2.4 Tensile testing

All samples underwent tensile testing using an MTS Landmark servo-hydraulic system, located in Eden Prairie, US, with a force capacity of 10 kN. The system features threaded grips where the specimens are securely held. Additionally, a 30mm axial clip extensometer from MTS was utilized, as depicted in Figure 2. Machining of the samples followed the guidelines outlined in the ASTM E8 standard. To ensure consistent testing conditions, the crosshead displacement speed was set at 0.476 mm/min. For each condition and orientation, the mechanical properties were determined based on the average results obtained from either four or six specimens, as illustrated in Figure 3. The stress-strain diagram of each specimen was used to calculate its individual mechanical properties. Yield stress measurements were determined using a 0.2% strain offset method. The As-built and HIP conditions comprised four specimens per sample, while the T6, HIP+T6, and SR1 conditions included six specimens per sample.

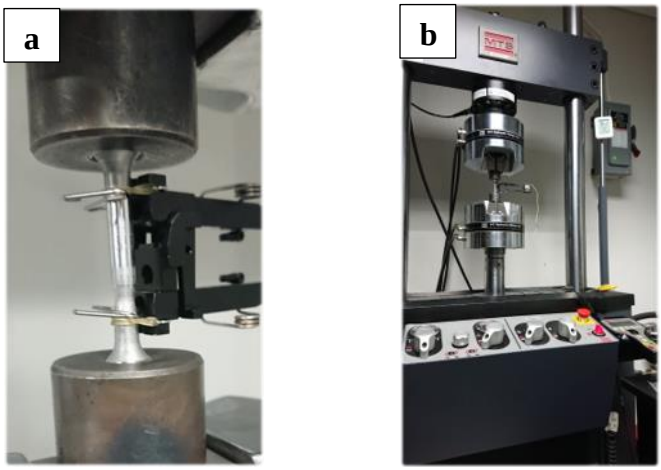

Figure 2. a) Tensile test performing sample, b) MTS Landmark servo-hydraulic system

2.5 Density measurements

Density measurements were conducted using the helium gas displacement method employing an Accupyc II 1340 Pycnometer from Norcross, United States. Each experimental variant underwent 10 measurements using the pycnometer. Mass measurements, on the other hand, were obtained utilizing a Sartorius CP124S weight balance manufactured by Sartorius AG in Germany. By combining the obtained mass and volume measurements, the density values were calculated.

2.6 Hardness measurement[AEG1]

Hardness testing was conducted in accordance with ASTM E384-17 standards using a Qatm - Qness 30 CHD Master+ instrument. The Vickers (HV) scale was utilized for the measurements. Samples that were printed in the vertical (Z) direction were evaluated, and measurements were taken from the X, Y, and Z planes. For each sample, five indentations were made on the surface using a load of 100gf. The indentations were spaced at least three millimeters apart.

3 RESULTS AND DISCUSSION

3.1 Microstructure and mechanical property comparisons

Figure 4 compares the light (optical) microscope images for unaged, Z-direction, as-built, SR1 treated, HIP, T6, and T6 + HIP treatment for EOS LPBF fabricated AlSi7Mg alloy components. The corresponding, representative stress-strain diagrams for each condition (Figure 4 (a) to (e)) are also shown in Figure 4 (f). The initial, as-built microstructure shown in Figure 4(a) is characterized primarily by ~1-micron micro dendritic cells which are altered at the interlayer melt bands. This microstructure is little altered after SR1 anneal at 285 ^{o}C (Figure 4(b)). The T6 (at 530 ^{o} C); roughly 0.8 melting point (~ 615 ^{o} C) treated components as shown in Figure 4(c) completely recrystallizes the dendritic microstructures in Figure 4(a) and (b), creating an average grain size of ~15 microns. This recrystallized grain structure contains a fairly homogeneous distribution of mostly coarse, eutectic Si particles having sizes as large as 5 microns (Figure

4(c)). Following HIP treatment at 515 ºC as shown in Figure 4(d), these Si particles have a wider size distribution, and higher particle density. The particles are more globular and the interparticle spacing is ~1 micron. The corresponding stress-strain diagram shown in Figure 4(f) illustrates a decrease in the YS and UTS, and a corresponding increase in the ductility (elongation) for the HIP treatment in contrast to the as-built, SR, and T6 treated components. These results were also observed for previous studies for LPBF fabrication and heat treatment of AlSi10Mg alloy [24-26]. The as-built alloy components following HIP + T6 treatment as shown in Figure 4(e) also exhibit a coarse Si particle size smaller than the HIP Si particles in Figure 4(c) as a result of the T6 treatment following the HIP treatment. The particle density and interparticle spacing is similar to those in Figure 4(c) for the T6 treatment.

It is useful to examine Figures 5 and 6 simultaneously since they represent the as built and heat treated AlSi7Mg components in Figure 4 following aging for 100 h and 1000 h at 140 ºC, respectively. It is apparent that not only are the component microstructures in Figures 5 and 6 essentially the same, but they are also little changed from those observed in Figure 4; with the exception of the HIP + 1000 h aging at 140 ºC (Figure 6 (d)), where the distribution of Si particles is denser. Indeed, the stress-strain diagrams in Figures 5(f) and 6(f) also exhibit essentially the same extremes between the as-built, SR, and HIP treated components as shown in Figure 4 (f). It is notable that the alloy components post-processed by HIP and aged for both 100 h and 1000 h at 177 ºC show very dense distributions of the eutectic Si particles: Figures 7(d) and 8(d), respectively. The corresponding stress-strain diagrams shown in Figures 7(f) and 8(f) are also similar and are templates of those stress-strain diagrams shown in Figures 4(f) to 6(f), especially for the HIP treatment. It might be noted that the eutectic Si particles in all cases are smaller, denser, and have a smaller interparticle spacing for HIP treatment in contrast to either T6 or HIP + T6 treatments: compare Figures 4(d) to 8(d) with Figs 4 to 8(c) and (e). This may represent an anomaly in part since smaller-spaced particles in general raise the strength and lower the ductility (elongation); opposite to the HIP-related stress-strain diagrams especially in contrast to those for the T6 and HIP + T6 treatment diagrams. However, in this case, the very large and irregular Si particles noted for the T6 and HIP + T6 treated components tend to act in a very different way, possibly emulating a duplex structure in connection with the small grains (~ 12-15 microns in contrast to 5-micron Si particles). This would give rise to a higher strength and lower ductility for the T6 and HIP + T6 components shown in the respective stress-strain diagrams [27]. It is notable that this phenomenon was also observed in our previous study of LPBF -fabricated and heat treated AlSi10Mg [24], where other related complexities of precipitation hardening were discussed.

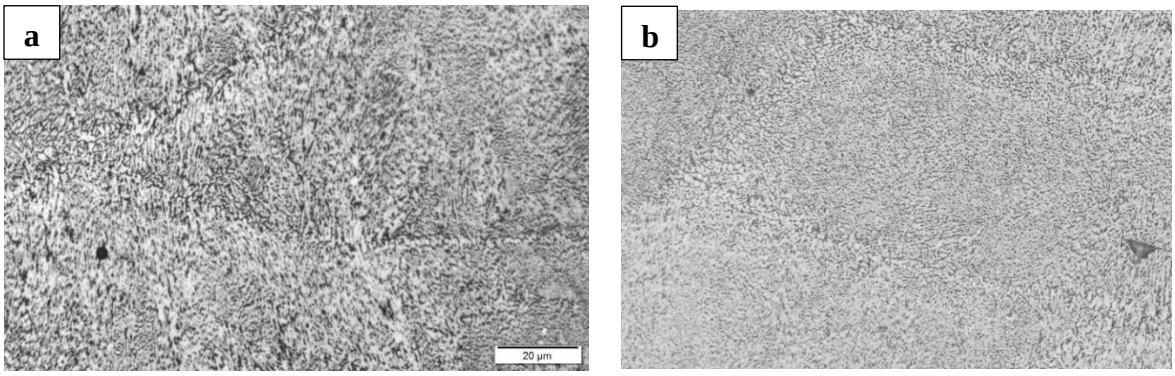

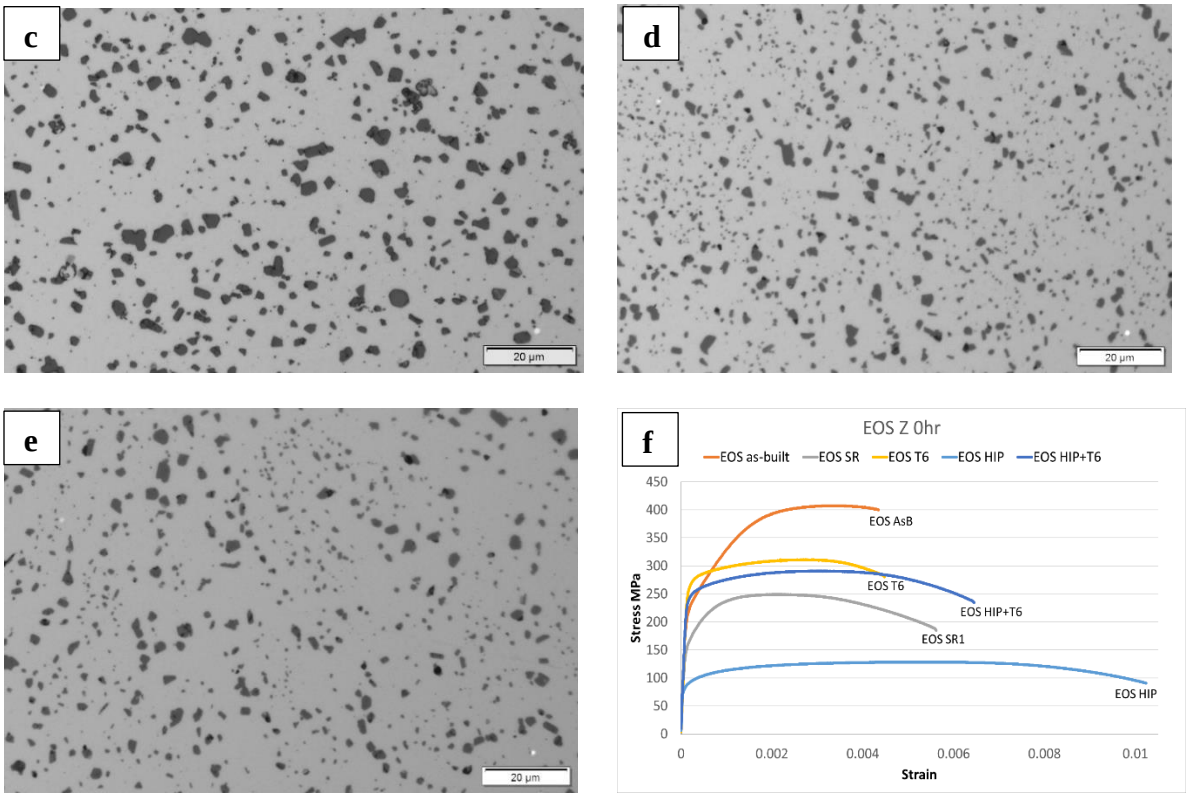

Figure 4. Microstructure images and corresponding stress-strain diagram for EOS F357 z-axis built and post process heat treatments with no aging. A) As built, b) SR1 c) T6, d) HIP, e) HIP+T6, f) Stress-strain diagram.

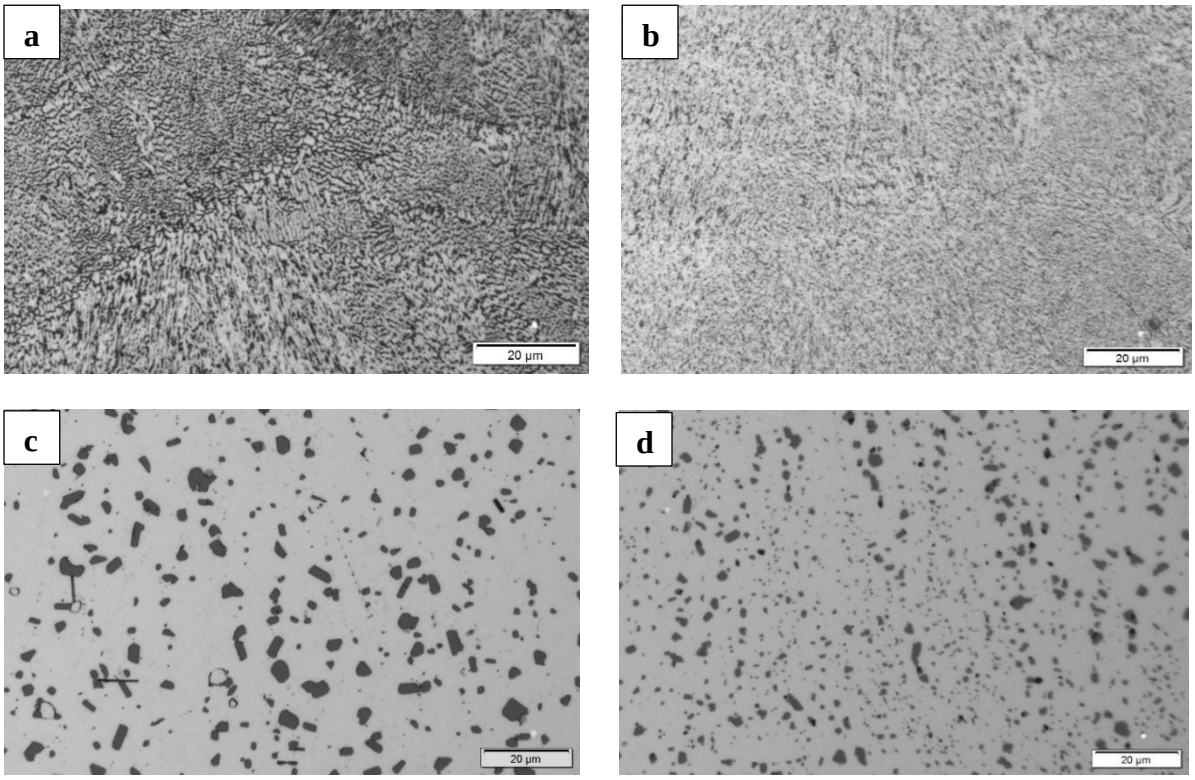

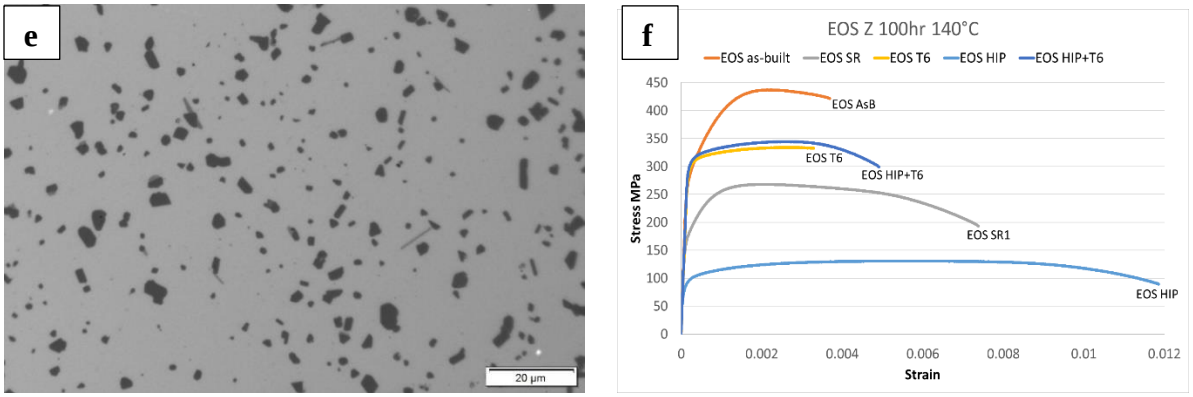

Figure 5. Microstructure images and corresponding stress-strain diagram for EOS F357 z-axis built and post process heat treatments aged for 100h at 140°C. a) As built, b) SR, c) T6, d) HIP, e) HIP+T6, f) Stress-strain diagram.

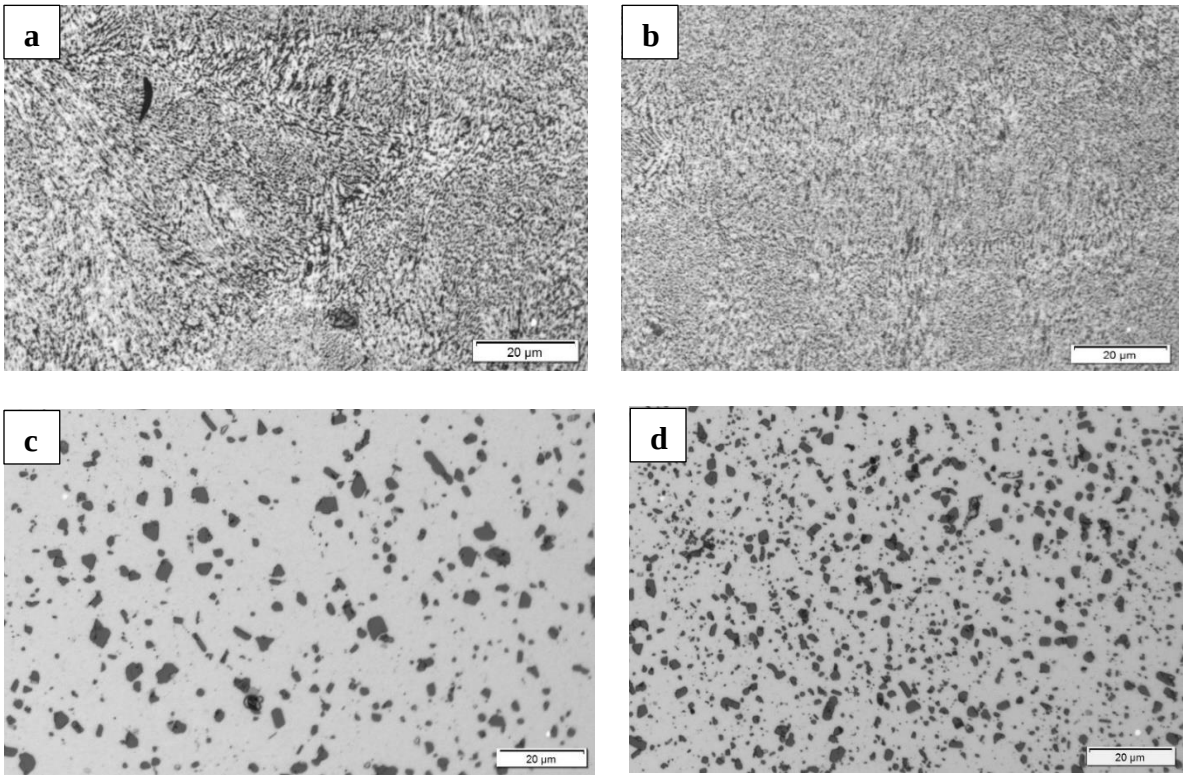

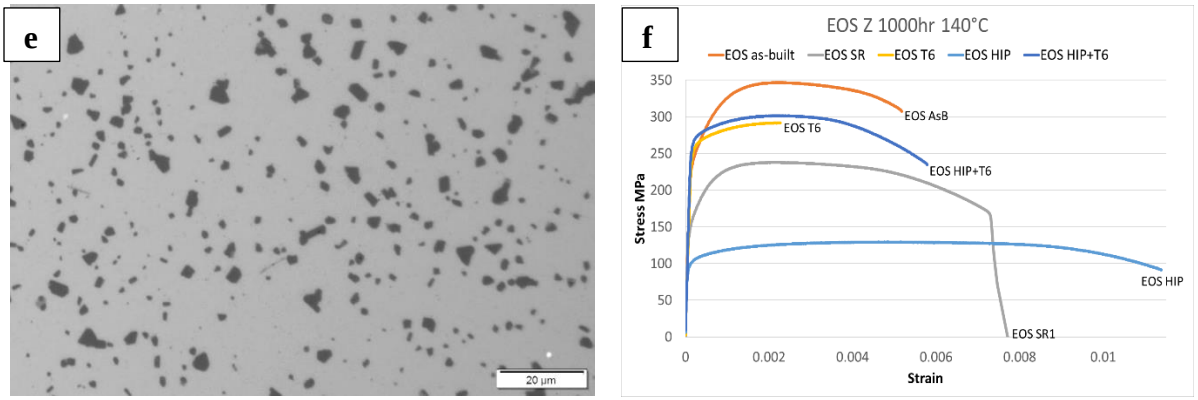

Figure 6. Microstructure images and corresponding stress-strain diagram for EOS F357 z-axis built and post process heat treatments aged for 1000h at 140°C. a) As built, b) SR1 c) T6, d) HIP, e) HIP+T6, f) Stress-strain diagram.

While Figures 4 to 8 only represent the range of microstructures and tensile (stress-strain) properties observed for EOS system-fabricated and post-process heat treated AlSi7Mg alloy components with and without aging treatments corresponding to the Z or build direction, components similarly fabricated and post-processed in the XY direction (perpendicular to the build direction as shown in Figure 3) produced essentially identical sequences of microstructures and corresponding stress-strain diagrams. In addition, components fabricated in the SLM LPBF system also produced the same microstructures and stress-strain diagram trends as those observed for the EOS system fabrications in both the Z and XY directions (Figure 3). Figure 9 provides support for this contention by comparing the stress-strain diagrams for both the EOS and SLM system components fabricated in both loading directions (Z and XY) and heat treated without aging. It is notable in Figure 9 that the extremes in the stress-strain diagrams show uniformly that the as-built components have the highest strength (YS and UTS) and lowest elongation to fracture while the HIP components exhibit the lowest strength and highest elongation to fracture, consistent with previous studies [24-26]. Note also that the trends of the stress-strain diagrams in Figure 9 are essentially the same for both the EOS system and SLM system fabricated AlSi7Mg components.

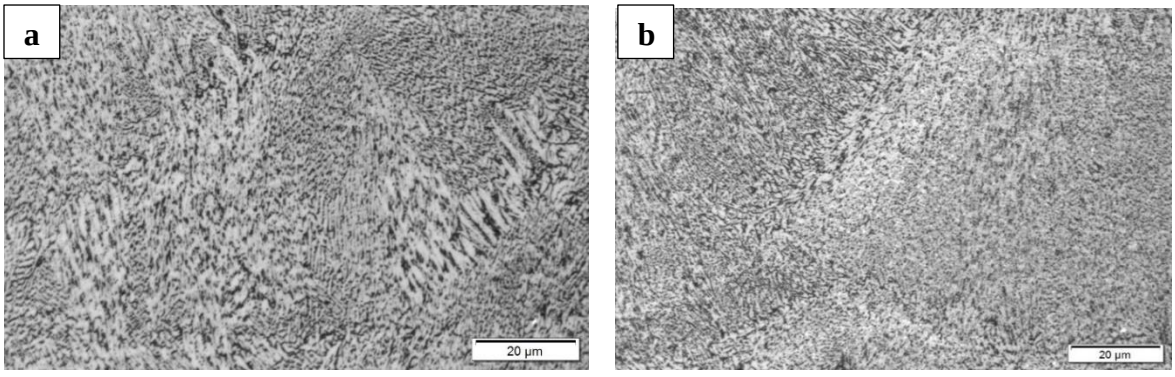

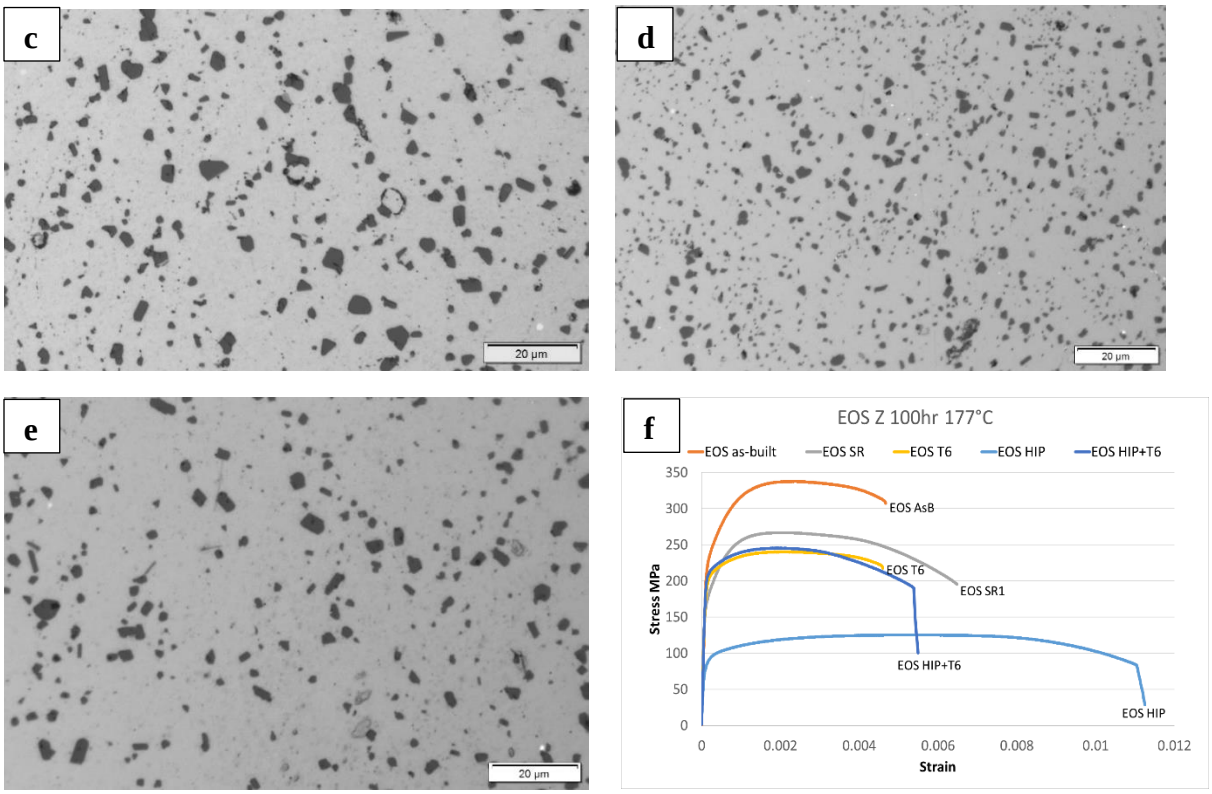

Figure 7. Microstructure images and corresponding stress-strain diagram for EOS F357 z-axis built and post process heat treatments aged for 100h at 177°C. a) As built, b) SR, c) T6, d) HIP, e) HIP+T6, f) Stress-strain diagram.

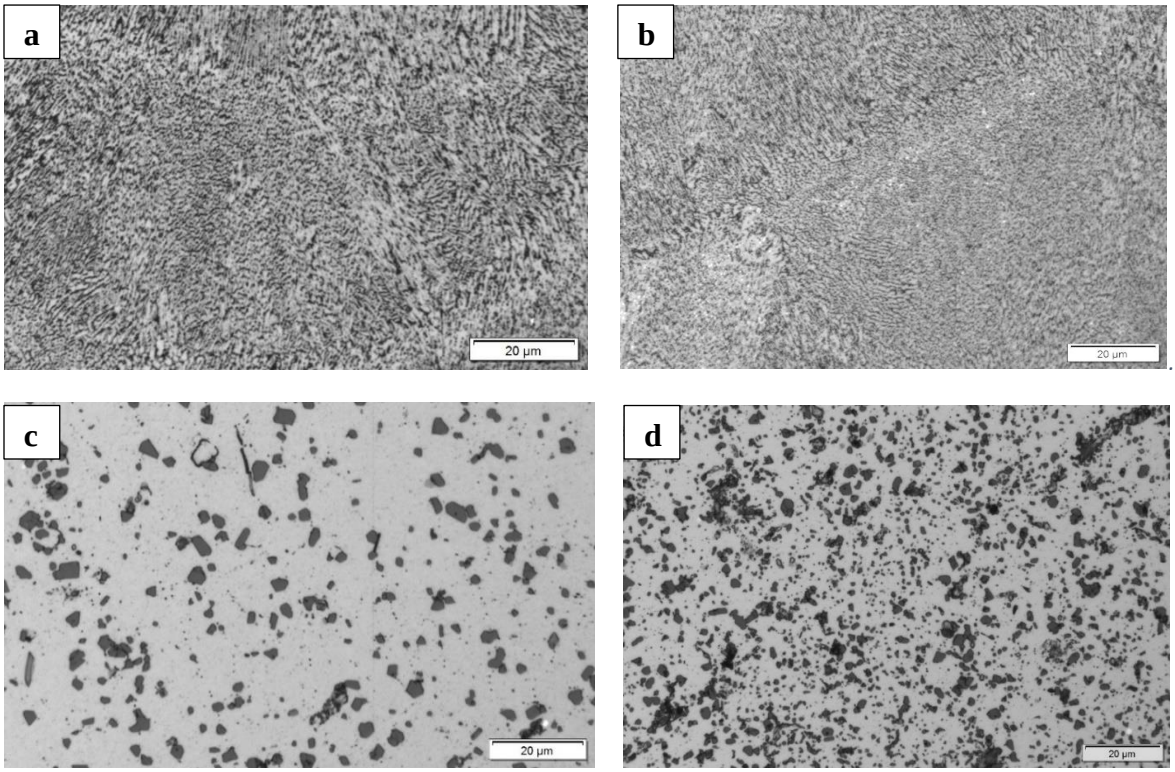

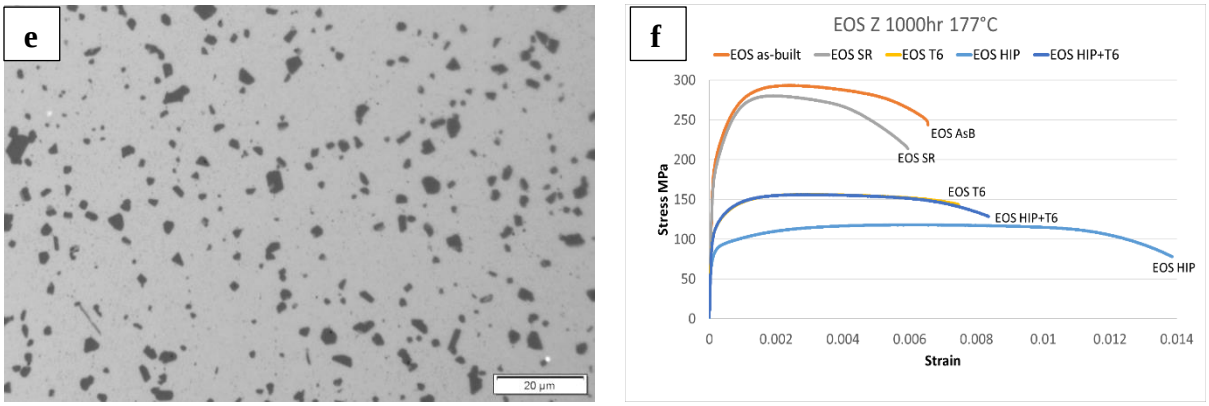

Figure 8. Microstructure images and corresponding stress-strain diagram for EOS F357 z-axis built and post process heat treatments aged for 1000h at 177°C. a) As built, b) SR, c) T6, d) HIP, e) HIP+T6, f) Stress-strain diagram.

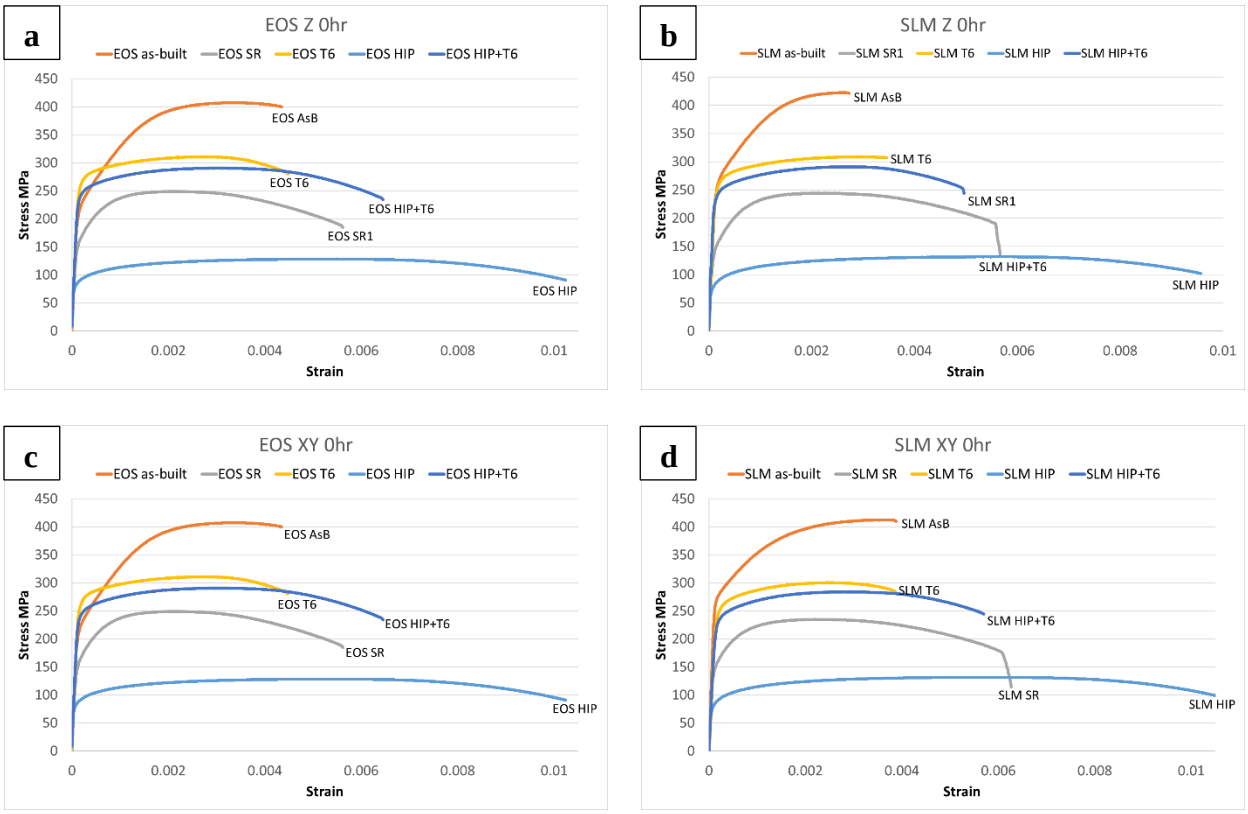

Figure 9 Characteristic curves for a) EOS printed parts in Z orientation, b) SLM printed parts in Z orientation, c) EOS printed parts in XY orientation and d) SLM printed parts in XY orientation.

Figure 10 represents alternative comparisons of stress-strain diagrams for components fabricated in the EOS system and aged along the left-hand portion of the figure (Figure10 (a), (c), (e), and (g), in contrast to corresponding SLM-fabricated components along the right-hand column (Figure 10 (b), (d), (f), and (h)), respectively. Here again there is a similarity in the trends of the individual stress-strain curves. A notable difference between these diagrams is their shape as

they tend to fracture for the SR-treated components in Fig 10 (e) and (g) for the EOS system and Figure 10 (f) and (h) for the SLM system; representing tensile testing in the Z and XY directions, respectively. This steep decline in stress over a narrow strain window is indicative of rapid thermal softening or necking as a result of a rapid increase in void fraction leading to failure. This phenomenon has been discussed in some detail by Pineau, et al. [28] and Wcislik and Pala [29] for metal failure in general.

Figures 11 and 12 illustrate that there is a preponderance of this steep softening for HIPed and aged tensile components fabricated in the Z and XY directions in both the EOS and SLM systems; especially notable in the XY direction as shown in Figure 12 (a) and (b). These results indicate that in some applications, components of AlSi7Mg alloy fabricated in the XY direction in either the EOS or SLM systems may pose some concerns after HIP and adding, which create a broader range of lower strengths in contrast to other heat treatments.

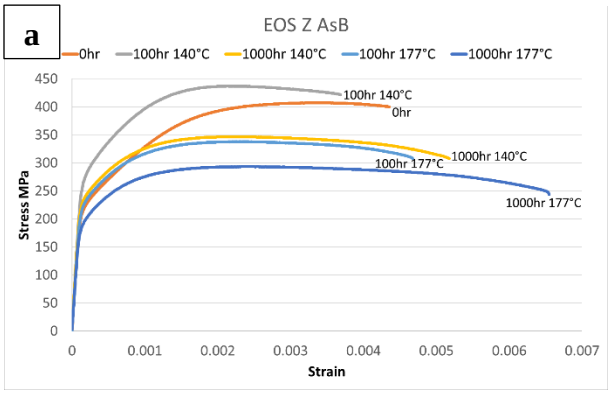

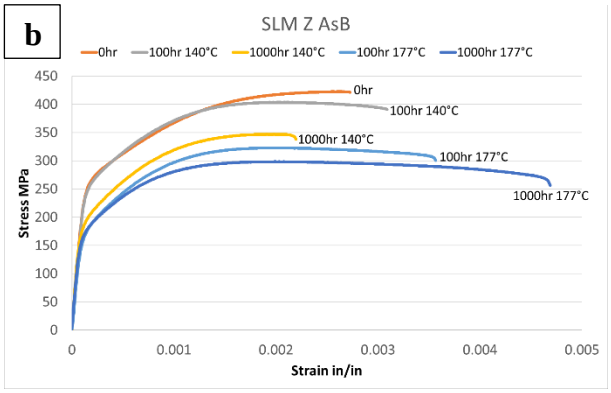

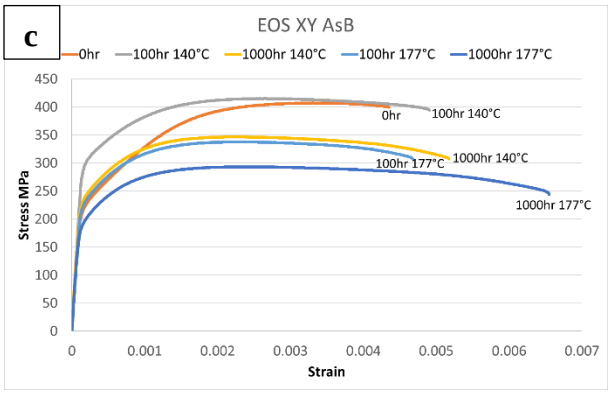

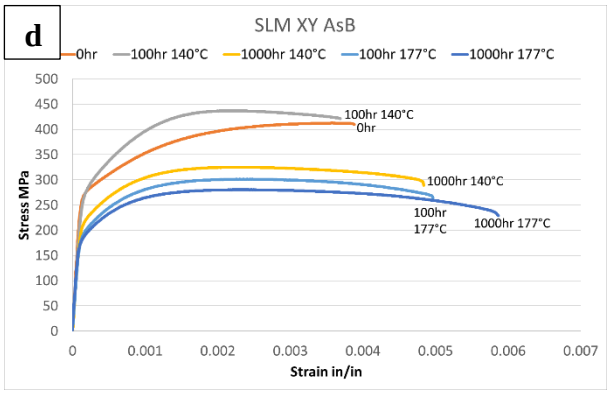

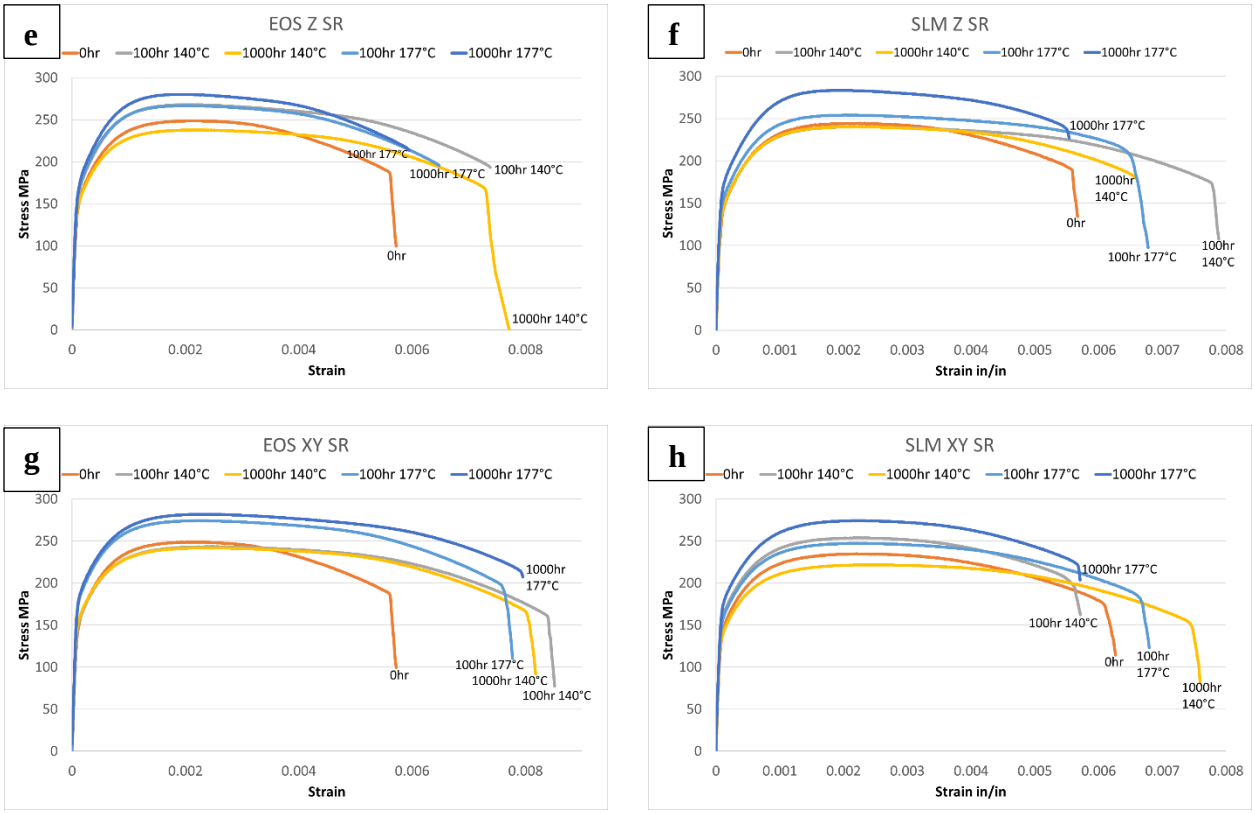

Figure 10. Characteristic curves for printed parts on a) EOS Z as built, b) SLM Z as built, c) EOS XY as built, d) SLM XY as built, e) EOS Z stress relief, f) SLM Z stress relief, g) EOS XY stress relief, h) SLM XY stress relief

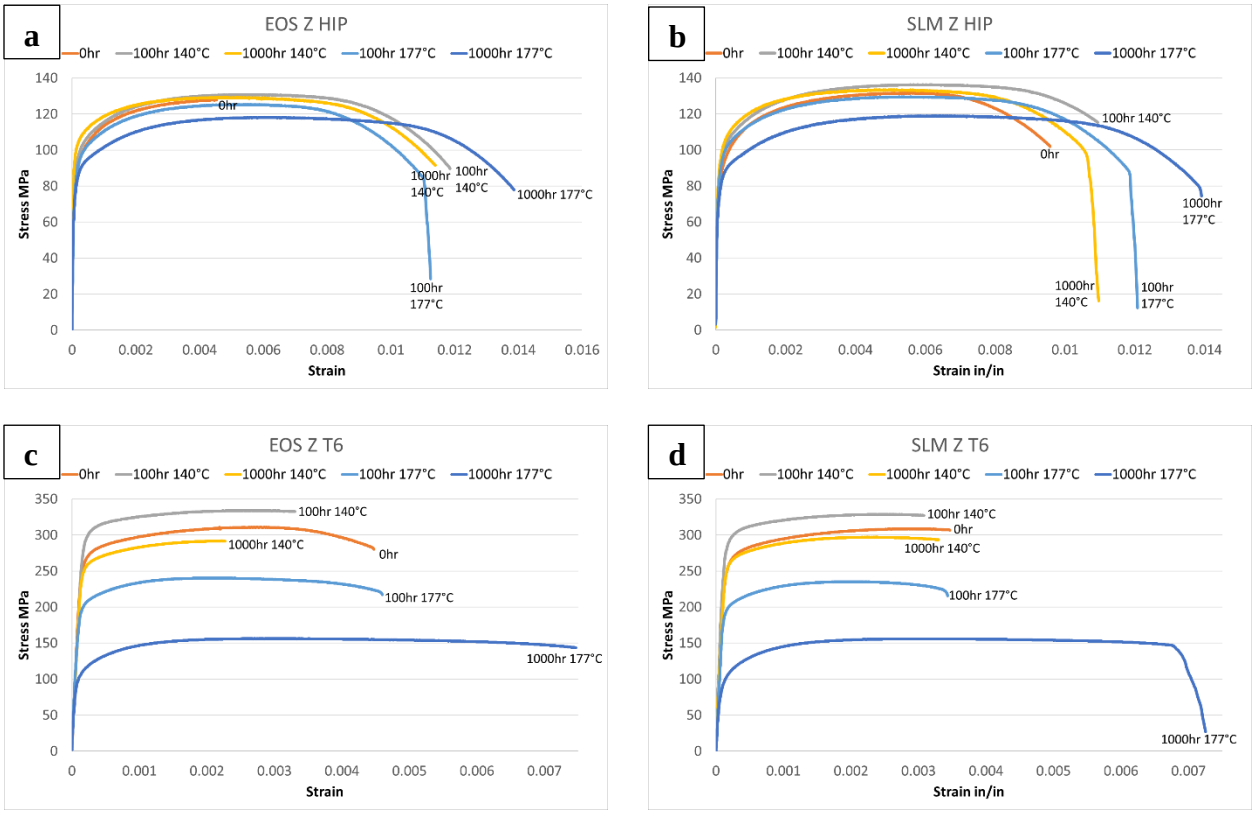

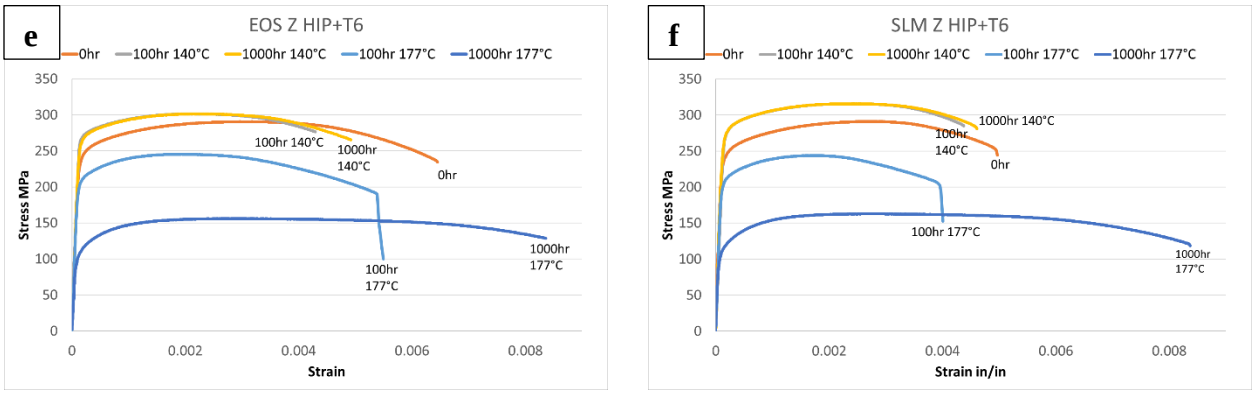

Figure 11. Characteristic curves for printed parts on a) EOS Z HIP, b) SLM Z HIP, c) EOS Z T6, d) SLM Z T6, e) EOS Z HIP+T6, f) SLM Z HIP+T6.

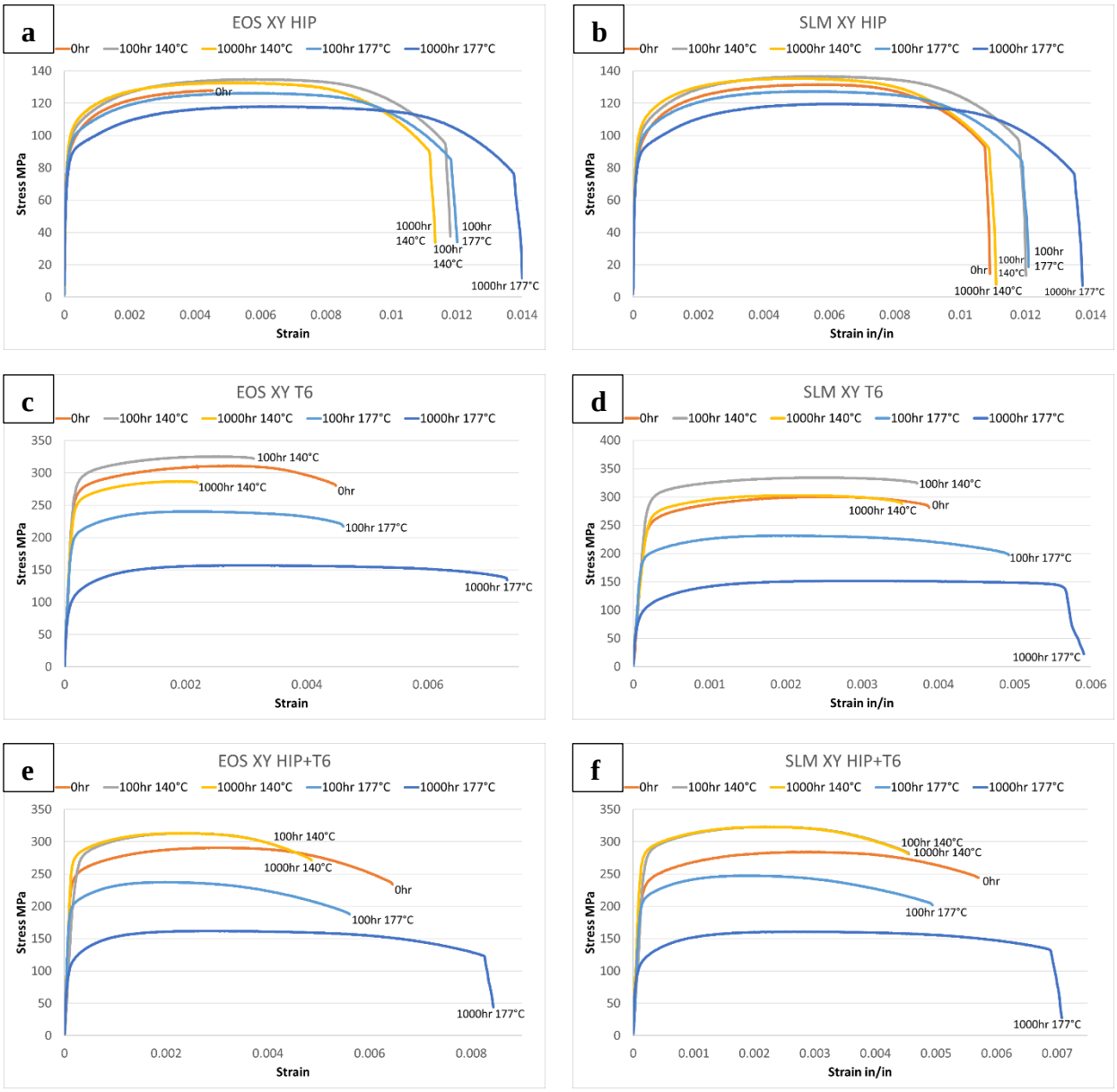

Figure 12. Characteristic curves for printed parts on a) EOS XY HIP, b) SLM XY HIP, c) EOS XY T6, d) SLM XY T6, e) EOS XY HIP+T6, f) SLM XY HIP+T6

3.2 Mechanical property comparisons and discussion

While the representation of tensile properties-yield stress (YS), ultimate tensile strength (UTS) and elongation (%)-as represented in the various comparative stress-strain diagrams in Figures 4 to 12 represent useful graphic overview and summaries of the variously heat treated (and aged) AlSi7Mg alloy components, the actual measured values are not obvious. Tables 4 to 7 list the average, measured mechanical property values (YS, UTS and elongation); including densities and microindentation hardness (HV) values for the various components. It can be observed in Tables 4 to 7, and as noted in the various stress-strain diagram comparisons, that the as-built

Table 4. Mechanical properties and related data for as built, SR, HIP, T6 and HIP+T6 on EOS Z build direction

EOS (Z)						
Heat Treatment	Aging Condition	Avg. YS (Mpa)	Avg. UTS (MPa)	Avg Elongation (%)	Density (g/cm^3)	Hardness (HV)
As Built	0hr	225	410	13.2	2.65	120
	100hr 140°C	282	440	8.5	2.65	133
	1000hr 140°C	212	372	9.2	2.65	115
	100hr 177°C	196	348	8.3	2.66	104
	1000hr 177°C	193	327	10.1	2.65	106
SR	0hr	159	250	18.2	2.65	79
	100hr 140°C	177	272	17.5	2.64	82
	1000hr 140°C	160	246	18.1	2.65	79
	100hr 177°C	170	261	15.9	2.65	89
	1000hr 177°C	189	290	13.9	2.65	96
HIP	0hr	87	132	25.3	2.65	51
	100hr 140°C	88	133	35.4	2.63	50
	1000hr 140°C	97	131	34.9	2.66	52
	100hr 177°C	84	126	34.6	2.64	50
	1000hr 177°C	81	118	41.3	2.65	44
T6	0hr	263	312	14.2	2.62	107
	100hr 140°C	291	330	12.8	2.59	118
	1000hr 140°C	264	303	10.0	2.62	112
	100hr 177°C	201	237	14.2	2.66	88
	1000hr 177°C	104	158	22.9	2.63	58
HIP + T6	0hr	205	258	18.7	2.66	60
	100hr 140°C	309	350	15.7	2.66	123
	1000hr 140°C	278	316	15.9	2.66	109
	100hr 177°C	206	243	16.6	2.67	86
	1000hr 177°C	109	158	27.2	2.65	59

YS and elongation values are reversed for the HIP values: as-built YS values are ~ 3 times the HIP values while the elongations for as-built components are roughly half those for the HIP components. Additionally, the XY-built component YS and elongations are generally larger than corresponding as-built Z direction components, while the HIP component values are little changed, indicating more homogenized microstructures and corresponding mechanical properties. This applies to the components fabricated in either the EOS or SLM systems, Confirming that AlSi7Mg components fabricated, and heat treated from either LPBF system do not differ significantly in their mechanical properties.

It is also of interest to observe in Tables 4 to 7 that aging at 177 ^{o}C for 1000 h decreased both the yield stress and corresponding micro indentation hardness (HV) in contrast to the unaged condition for all as-built, HIPed, T6 and HIP + T6 treated components for both loading directions (Z and XY) for both LPBF systems (EOS and SLM); the exception being the SR-treated components where both the YS and HV values increased from the unaged condition.

It can also be observed that the trends in the associated micro indentation hardness (HV) values correspond to the YS values: high YS values for the as-built components correspond to high HV values while the low YS values for HIP components correspond the low HV values for these components. It is observed in Tables 5 to 7 that products fabricated in the XY direction have YS Values ~ 12% higher than those fabricated in the Z direction. In contrast, elongations for HIP components are generally similar to either Z or XY builds, although the highest elongations of ~ 40 % occur uniformly for HIP + aging at 177 ^{o}C for 1000 h.

Table 5. Mechanical properties and related data for as built, SR, HIP, T6 and HIP+T6 on SLM Z build direction

SLM (Z)						
Heat Treatment	Aging Condition	Avg. YS (Mpa)	Avg. UTS (Mpa)	Avg Elongation (%)	Density (g/cm^3)	Hardness (HV)
As Built	0hr	263	409	6.9	2.64	122
	100hr 140°C	271	411	8.3	2.65	125
	1000hr 140°C	202	350	9.3	2.65	106
	100hr 177°C	182	321	9.7	2.62	102
	1000hr 177°C	183	291	14.2	2.65	91
SR	0hr	156	253	16.3	2.65	80
	100hr 140°C	156	241	20.3	2.65	81
	1000hr 140°C	149	237	21.6	2.65	77
	100hr 177°C	158	251	19.7	2.65	81
	1000hr 177°C	177	279	16.8	2.65	89
HIP	0hr	85	135	31.3	2.65	51
	100hr 140°C	88	136	36.1	2.64	51
	1000hr 140°C	93	134	35.7	2.66	53
	100hr 177°C	88	130	36.5	2.62	48
	1000hr 177°C	80	119	41.8	2.65	47
T6	0hr	267	316	11.2	2.62	113
	100hr 140°C	292	330	10.3	2.57	113
	1000hr 140°C	268	299	10.9	2.63	110
	100hr 177°C	201	240	12.1	2.58	87
	1000hr 177°C	102	157	21.8	2.55	57
HIP + T6	0hr	199	258	19.2	2.67	65
	100hr 140°C	314	352	17.6	2.66	126
	1000hr 140°C	278	316	15.2	2.66	111
	100hr 177°C	212	238	14.4	2.65	81
	1000hr 177°C	111	160	24.3	2.65	58

Table 6. Mechanical properties and related data for as built, SR, HIP, T6 and HIP+T6 on EOS XY build direction

EOS (XY)						
Heat Treatment	Aging Condition	Avg. YS (Mpa)	Avg. UTS (MPa)	Avg Elongation (%)	Density (g/cm^3)	Hardness (HV)
As Built	0hr	257	410	17.2	2.65	122
	100hr 140°C	311	421	14.6	2.66	136
	1000hr 140°C	237	350	14.9	2.66	111
	100hr 177°C	218	325	16.0	2.65	110
	1000hr 177°C	199	298	20.1	2.67	97
SR	0hr	163	249	20.4	2.65	79
	100hr 140°C	170	252	23.8	2.66	90
	1000hr 140°C	162	228	24.5	2.66	81
	100hr 177°C	176	259	23.1	2.65	91
	1000hr 177°C	189	278	23.1	2.53	91
HIP	0hr	89	136	28.1	2.66	51
	100hr 140°C	92	137	36.0	2.64	48
	1000hr 140°C	95	135	35.6	2.67	51
	100hr 177°C	86	127	35.5	2.63	48
	1000hr 177°C	82	120	41.5	2.66	46
T6	0hr	263	315	12.8	2.62	109
	100hr 140°C	291	330	10.2	2.62	113
	1000hr 140°C	262	300	7.8	2.59	102
	100hr 177°C	204	242	14.2	2.59	86
	1000hr 177°C	104	150	17.8	2.58	55
HIP + T6	0hr	216	275	18.4	2.66	59
	100hr 140°C	301	348	15.1	2.67	119
	1000hr 140°C	281	320	13.6	2.64	105
	100hr 177°C	199	240	17.7	2.68	87
	1000hr 177°C	113	165	26.3	2.67	59

Table 7. Mechanical properties and related data for as built, SR, HIP, T6 and HIP+T6 on SLM XY build direction

SLM (XY)						
Heat Treatment	Aging Condition	Avg. YS (Mpa)	Avg. UTS (Mpa)	Avg Elongation (%)	Density (g/cm^3)	Hardness (HV)
As Built	0hr	295	412	13.1	2.65	133
	100hr 140°C	283	392	11.8	2.65	130
	1000hr 140°C	215	322	14.4	2.66	101
	100hr 177°C	196	303	14.7	2.65	95
	1000hr 177°C	188	285	16.5	2.67	93
SR	0hr	155	241	19.3	2.65	79
	100hr 140°C	164	234	18.0	2.65	81
	1000hr 140°C	148	226	21.4	2.65	74
	100hr 177°C	163	245	19.7	2.65	80
	1000hr 177°C	180	254	17.5	2.65	90
HIP	0hr	125	181	17.6	2.65	49
	100hr 140°C	90	139	36.0	2.57	49
	1000hr 140°C	95	137	32.6	2.66	49
	100hr 177°C	88	129	35.7	2.56	47
	1000hr 177°C	82	120	39.8	2.65	43
T6	0hr	260	311	12.9	2.63	107
	100hr 140°C	295	334	10.4	2.56	120
	1000hr 140°C	258	297	8.9	2.61	108
	100hr 177°C	197	235	14.1	2.59	81
	1000hr 177°C	103	156	19.8	2.67	56
HIP + T6	0hr	228	281	16.5	2.66	65
	100hr 140°C	309	352	15.9	2.66	122
	1000hr 140°C	286	326	13.9	2.67	111
	100hr 177°C	210	247	14.3	2.66	89
	1000hr 177°C	111	162	23.1	2.65	58

It should also be mentioned that the measured densities shown in Tables 4-7 vary from 2.53 g/cm^3 to 2.67 g/cm^3, but this spread in measured densities does not appear to have any systematic heat treatment basis and would appear to be primarily measurement error. There is correspondingly no correlation between the measured densities and the associated mechanical properties, including the micro indentation hardness. It might be noted that solution treatments of AlSi10Mg at 540 ^{o}C reduced the density as a result of diffusion of dissolved hydrogen and increasing gas porosity in a study by Girelli, et al. [30]. However, there is no evidence of these phenomena in the present study.

While Tables 4 to 7 provide a comprehensive matrix for design strategies and mechanical property selection for LPBF-fabricated AlSi7Mg alloy products, the trending of properties, particularly mechanical properties, are difficult to compare, even including the stress-strain diagram comparisons shown in Figures 4 to 12. While it may seem overly redundant, we have

prepared a series of comparative and systematic bar graph summaries illustrating the heat-treatment regimens and corresponding aging treatments for AlSi7Mg alloy fabricated in both the EOS and SLM LPBF systems, and in both the Z and XY loading directions, relative to the build direction. These are shown in Figures 13 and 14. It is interesting to observe that these two comparative figures, representing each LPBF system (EOS and SLM) are essentially templates of one another; illustrating essentially the same trending as discussed extensively above. It can also be noted that Figure 13 for the EOS system is a template for the same heat treatment schedule trends determined for LPBF fabrication of AlSi10Mg alloy components reported in Figure 5 of our previous article [24]. It is also observed that the as-built and as-built and aged components in Figures 13 and 14 exhibit a reversed trend for YS and UTS versus elongation, in contrast to HIP and aged components: higher YS and UTS exhibit lower elongations while lower YS and UTS exhibit higher elongations.

It will be noted in retrospect that the Introduction in this study illustrated a range of prior research work describing post-process heat treatments for LPBF fabrication of AlSi10Mg alloy components [11,15,17,18-20,24]. However, far fewer studies have been reported for AlSi7Mg (F357) alloy [10,11]. Vanzetti, et al. [31] have recently described short heat treatments for F357 (AlSi7Mg) alloy processed by LPBF, and involving T6 treatment and direct aging. They observed an optimized yield stress of 308 MPa and an elongation of only 3.9 %; nearly 1/3 of the present as-built elongations having similar yield stress values. Similarly, Fiocchi, et al. [32] in their recent review of heat treatment of LPBF-fabricated aluminum alloys noted that thermal treatment of AlSi7Mg alloy actually reduced the as-built elongation from 7.6 % to 4.7 % at a relatively constant yield stress of 257 MPa; less than half the elongation at the same yield stress in the present study (see Tables 4 to 7). In a recent paper by Pezda [10] dealing with the optimization of T6 heat treatment parameters of cast AlSi7Mg alloy where elongations increased by 250 % at aging above 300^{o}C; characteristic of HIP treatment and aging as shown in the current study Correspondingly, there are few prior reports involving HIP of LPBF-fabricated AlSi7Mg alloy. A recent study by Oliveira de Menezes, et al. [33] for LPBF fabrication of AlSi7Mg alloy examined the effect of heat treatment parameters and loading orientation on the tensile properties. This study pointed out that while there is a notable anisotropy in mechanical properties between components built parallel and perpendicular to the build direction (Z), this can be reduced or eliminated by heat treatment (such as T6 temper) as observed for numerous other aluminum alloys [11-13, 22,24], as well as many other metals and alloys [34,35]. Indeed, it is observed in the current study (Tables 4-7) that AlSi7Mg alloy components built in both the EOS and SLM LPBF systems exhibit yield stress values (YS) in the Z (vertical) and XY (horizontal) loading directions of 225 MPa and 263 MPa, and 257 MPa and 295 MPa, respectively: an anisotropy of ~ 16%. However, after T6 treatment for example, the values become 263 MPa for both directions in the EOS system, and 267 MPa and 260 MPa for the Z and XY directions, respectively in the SLM system.

Figure 13. Comparative bar graphs showing mechanical properties for F357 on EOS printer, under different aging conditions for the different heat treatments and built in Z and XY orientation, a), d) Yield strength, b), e) UTS and c), f) Elongation; notice strength decreases with aging in a), b), d) and e), while elongation increases in c) and f) for T6, HIP and HIP+T6.

Figure 14. Comparative bar graphs showing mechanical properties for F357 on SLM printer, under different aging conditions for the different heat treatments and built in Z and XY orientation, a), d) Yield strength, b), e) UTS and c), f) Elongation; notice strength decreases with aging in a), b), d) and e), while elongation increases in c) and f) for T6, HIP and HIP+T6.

4 SUMMARY AND CONCLUSIONS

This research program is a comprehensive investigation into the fabrication and heat treatment of AlSi7Mg (F357) alloy using laser powder bed fusion (LPBF). Tensile specimens were fabricated in the Z (build) and XY loading directions on two LPBF systems: EOS M290 and SLM 280HL. The components underwent aging for 100 hours and 1000 hours at temperatures of 140°C and 177°C, respectively. Heat treatment processes included stress relief (SR1) anneal, hot isostatic pressing (HIP), T6 treatment, and HIP + T6 treatment.

A total of 1660 measurements were conducted, including yield stress (YS), ultimate tensile strength (UTS), elongation, and micro indentation hardness (HV). Density measurements were also performed. The mechanical properties exhibited anisotropy between the Z and XY loading directions for each LPBF system. For example, the unaged YS of EOS (Z) was 225 MPa, while EOS (XY) had a YS of 257 MPa. Similarly, the unaged YS of SLM (Z) was 263 MPa, whereas SLM (XY) had a YS of 295 MPa.

The highest YS values were consistently observed for the T6 treatment + 100-hour aging at 140°C. For example, the EOS (Z) and (XY) components had YS values of 291 MPa and 292 MPa, respectively. Similarly, the SLM (Z) and (XY) components had YS values of 292 MPa and 295 MPa, respectively.

The micro indentation hardness (HV) measurements were consistent with EOS (Z) and EOS (XY) exhibiting hardness values of HV 120 and HV 122, respectively, while SLM (Z) and SLM (XY) had hardness values of HV 122 and HV 133, respectively.

These findings demonstrate the influence of heat treatment and aging on the mechanical properties of LPBF-fabricated AlSi7Mg (F357) alloy components, hence we can conclude the following:

* Although only two different LPBF systems (EOS and SLM) were compared in this study, it would appear that machine differences do not significantly alter AlSi7Mg alloy products produced, and any inhomogeneities and anisotropies are erased as a result of heat treatment, especially HIP, T6 and HIP + T6 treatments.

* As-built AlSi7Mg alloy products fabricated in the build (Z) direction varied in yield stress from 225 MPa to 295 MPa in this study; with corresponding elongation variations 0f 7 % to 17 %. These properties reflect the most economical and process efficient strategy.

* While HIP treatment can produce a homogenized microstructure even without aging, the resulting yield stress values were observed to vary from 85 MPa to 87 MPa for Z-direction fabricated components; with corresponding elongations varying from 25 % to 31 %. The highest elongation was observed for HIP + 1000 h aging at 177 ^{o}C: 42 %.

* Bar graph representations of the tensile properties (YS, UTS, elongation) for both the LPBF systems heat treated and heat treated + aging (as shown in Figures 13 and 14) were templates of one another.

REFERENCES

[1] Moller H, Govender G, Stumpf WE, Pistorius PC. Comparison of heat treatment response of semisolid metal processed alloys A356 and A357. Int J Cast Met Res 2010; 23: 37-43.

[2] Totten GE, editor. Heat treating aluminum and its alloys. Materials Park, OH: ASM International; 2016.

[3] Totten GE, Tiryakioglu M, Kessler O. editors. Encyclopedia of aluminum and its alloys. Boca Raton: CRC Press; 2018.

[4] Manente A, Timelli G. Optimizing the heat treatment process of cast aluminum alloys. In Recent trends in processing and degradation of aluminum alloys. Ahmad Z. editor. Rijeka, Croatia: InTech; 2011, pp. 181-203.

[5] Kaufman JG, Rooy E. Aluminum alloy casting, properties, processes and applications. Materials Park, OH: ASM International; 2004, pp. 27-31.

[6] Kordas P, Zyska A. The effect of heat treatment on mechanical properties of squeeze castings from AlSi7Mg alloys. In Proc 26th Int Conf Metall and Mater. Brno, Czech Republic: 24-26 May 2017; pp. 2694-2696.

[7] Czekaj E, Zych J, Kwak Z, Garbacz-Klempka A. Quality index of the AlSi7Mg0.3 aluminum casting alloy depending on the heat treatment parameters. Arch Foundry Eng 2016; 16:25-28.

[8] Birol Y. Impact of grain size on mechanical properties of AlSi7Mg0.3 alloy. Mater Sci Eng 2013; 559: 394-400.

[9] Moller H, Govender G, Stumpf W. Application of shortened heat treatment cycles on A356 automotive brake calipers with respective globular and dendritic microstructures. Trans Nonferr Net Soc China 2010: 20: 1780-1785.

[10] Pezda J. Optimization of heat treatment parameters of AlSi7Mg alloy. Mater 2022; 15:1163.

[11] Fiocchi J, Tuissi A, Biffi CA. Heat treatment of aluminum alloys produced by laser powder bed fusion: A review. Mater Design 2021: 204: 109651.

[12] Rometsch PA, Zho Y, Wu X, Huang A. Review of high- strength aluminum alloys for additive manufacturing by laser powder bed fusion. Mater Design 2022: 219: 110779.

[13] Cao Y, Lin X, Wang QZ, Shi SQ, Ma L, Kang N, Huang WD. Microstructure evolution and mechanical properties at high temperature of selective laser melting AlSi10Mg. J Mater Sci Tech 2021: 62: 162-172.

[14] Tang H, Gao C, Zhang Y, Zhang N, Lei C, Bi Y, Tang P, Rao JH. Effects of direct aging treatment on microstructure, mechanical properties and residual stress of selective laser melted AlSi10Mg alloy. J Mater Sci Technol 2022: online Oct 14.

[15] Jiang X, Xiong W, Wang L, Guo M, Ding Z. Heat treatment effects on microstructure-residual stress for selective laser melting AlSi10Mg. Mater Sci Technol 2020: 36(2): 168-180.

[16] Alboulkhair NT, Simonelli M, Perry L, Ashcroft I, Tuck C. 3D printing of aluminum alloys, additive manufacturing of aluminum alloys using selective laser melting. Prog Mater Sci 2019:106: 100578.

[17] Ertugrul O, Oter ZC, Yilmaz MS, Sahin E, Coskun M, Tarakci G, Koc E. Effect of HIP process and subsequent heat treatment on microstructure and mechanical properties of direct metal laser sintered AlSi10Mg alloy. Rapid Prototyp J 26 June 2020.

[18] Zhuo L, Wang Z, Zhang H, Yin E, Wang Y, Xu T, Li C. Effect of post-process heat treatment on microstructure and properties of selective laser melted AlSi10Mg alloy.

Mater Lett 2019: 234: 196-200.
[19] Casati R, Nasab MH, Coduri M, Tirelli V, Vedani M. Effects of platform pre-heat and thermal-treatment strategies on properties of AlSi10Mg alloy processed by selective laser melting. Metals 2018: 8: 954(8110954).
[20] Takata N, Kodaira H, Sekizawa K, Suzuki A, Hobashi M. Change in microstructure of selective laser melted AlSi10Mg alloy with heat treatments. Mater Sci Eng2018: 143: 18-26.
[21] Alghamdi F, Song X, Hadadzadeh A, Shalehi-Amirkhiz B, Mohammadi M, Haghshenas M. post heat treatment of additive manufactured AlSi10Mg: On silicon morphology, texture and small-scale properties. Mater Sci Eng 2020: 783: 139296.
[22] Sert E, Ochsner A, Hitsler L, Werner E, Merkel M. Additive manufacturing: A review of the influence of building orientation and post heat treatment on the mechanical properties of aluminum alloys. In: State of the art and future trends in material modelling, Altenbach H, Ochsner A editors, New York, Springer 2019, pp 349-366.
[23] Michi RA, Plotkowski A, Shyam A, Dehoff RR, Babu SS. Towards high-temperature applications of aluminum alloys enabled by additive manufacturing. Int Mater Rev 2022: 67(3): 298-345.
[24] Merino J, Ruvalcaba B, Varela J, Arrieta E, Murr LE, Wicker RB, Benedict M, Medina F. Multiple, comparative heat treatment and aging schedules for controlling the micro structures and mechanical properties of laser powder bed fusion fabricated AlSi10Mg alloy. J Mater Res Technol 2021; 13: 669-685.
[25] Finfrock CB, Exil A, Carroll JD, Deibler L. Effect of hot isostatic pressing and powder feed stock on porosity, microstructure, and mechanical properties of selective laser melted AlSi10Mg. Metall Microstruct Anal 2018; 7: 443-456.
[26] Zhang C, Zhu H, Qi Y, Zeng X. The effect of annealing on microstructure and mechanical properties of selective laser melting of AlSi10Mg. IOF Conf series: Mater Sci Eng 2019; 538: 012023.
[27] Horiuchi T, Satoh N. Relationship between duplex grain structure and grain boundary precipitates in N_2M-stabilized alloy. E-J Adv Maint 2013; 5: 165-17427].
[28] Pineau A, Benzerga AA, Pardoen T. Failure of metals I: brittle and ductile fracture. Acta Mater 2016; 107:424-483.
[29] Wcislik W, Pala K. Some microstructural aspects of ductile failure of metals. Mater 2021; 14:4321.
[30] Girelli L, Tucci M, Montesano L, Gelfi M, Pola A. Optimization of heat treatment parameters for additive manufacturing and gravity casting of AlSi10Mg alloy. IOP Conf Ser Mater Sci Engr 2017; 264: 012016.
[31] Vanzetti M, Virgillito E, Aversa A, Manfredi D, Bondioli F, Lombardi M, Fino P. Short heat treatments for F357 aluminum alloy processed by laser powder bed fusion. Mater 2021; 14:6157.
[32] Fiocchi J, Tuissi A, Biffi CA. Heat treatment of aluminum alloys produced by laser powder bed fusion: A review. Mater Design 2021; 204: 109651.
[33] Oliveira de Menezes, JT, Castrodeza EM, Patriarea L, Casati R. Effect of heat treatments and loading orientation on tensile properties and fracture toughness of AlSi7Mg alloy produced by laser powder bed fusion. Int J Fracture 2022; 235:145-157.
[34] Amato KN, Hernandez J, Murr LE, Martinez E, Gaytan SM, Shindo PW. Comparison of microstructures and properties for a Ni-base superalloy (alloy 625) fabricated by electron

and laser beam melting. J Mater Sci Res2012; 1(3):41 pp.
[35] DebRoy T, Wei HL, Zubeck JS, Mukherjee T, Elmer JW, Milewski JO, Beese AM, Wilson-Heid A, De A, Zhang W. Additive manufacturing of metallic components-process, structure, and properties. Prog Mater Sci 2018; 92:112-224.
[36] Qin W, Li J, Liu Y, Zhu L, Shu D, et al. Effects of grain size on tensile property and Fracture morphology of 316L stainless steel. Mater Lett 2019; 254:116-119.
[37] Liu BB, Han JQ, Zhao R, Liu W, Wan M. Grainsize effect on fracture behavior of the axis-Tensile test of Inconel 718 sheet. High Temp Mater Proc 2016; 35(10): 989-998.
[38] Sun Y, Yu X, Ge D, Chen J. Fracture morphologies by advanced high strength steel during deformation. Acta Metall Sin 2014; 27(1): 101-106.
[39] Das A, Trafder S. Geometry of dimples and its correlation with mechanical properties of Austenitic stainless steels. Scripta Mater 2008; 59(9): 1014-1017.
[40] Hilders OA, Zambrano N, Caballero R. Microstructure, strength and fracture topography in AISI 304L stainless steel as seen through a fractal approach and Hall-Petch law. Int J Metals 2015; 10: 624653.
[41] Manjunath GK, Preetham Kumar GV, Bhat KU. Tensile properties and tensile fracture characteristics of cast Al-Zn-Mg alloys processed by equal channel angular pressing. Trans Indian Inst Met 2017; published online Feb. 17, 10 pp.

ACKNOWLEDGEMENTS

Primary support for this research was provided by grant number NOAID20210005 from AFRL (Air Force Research Laboratory) as well as strategic investments via discretionary UTEP Keck Center funds and the Mr. and Mrs. MacIntosh Murchison Chair I in Engineering Endowment at UTEP. The research described here was performed at The University of Texas at El Paso (UTEP) within the W.M. Keck Center for 3D Innovation (Keck Center). The authors are grateful to Jorge Merino for its guidance in the writing of this paper. The views and opinions expressed in this article are those of the authors and do not necessarily reflect the official opinion or policy of any agency of the US government (if applicable).